利用光轴可移动液晶透镜的立体图像采集系统

万超杰[1]，刘志强[1]，徐律涵[1]，李慧海[2]，叶茂[1*]

[1]电子科技大学光电科学与工程学院，四川 成都 611731；
[2]四川天微电子股份有限公司，四川 成都 610200

摘要　针对传统双目视觉系统体积大、成本高等缺点，提出了一种利用光轴可移动液晶透镜的单相机立体图像采集系统。该系统由一个固定的相机模块和一个贴有偏振片的液晶透镜构成。通过改变电压的方式移动光轴并采集图像，利用光流法获取图像视差。研究了液晶透镜光轴变化对系统整体光轴的影响，推导了视差与深度的关系。通过验证所采集的图像存在视差来说明所设计系统的可行性，并进行了近距离物体的深度获取。实验结果表明，利用液晶透镜的光轴移动功能可以使系统的整体光轴产生移动，实现立体视觉。所设计系统无需机械移动，具有结构简单紧凑和成本低廉的优点，为立体图像的采集提供了新的方法。

关键词　成像系统；液晶透镜；光轴移动；图像采集；深度获取

中图分类号　TN141.9　　　**文献标志码**　A　　　　　　　　　　　　　　**DOI**：10.3788/AOS221402

1　引　言

立体图像采集系统旨在从物理世界中采集含有物体视差信息的图像，是深度获取的硬件支撑，对于现实世界的各种应用，如工业检测[1]、自主导航任务[2]等是非常重要的。立体图像通常通过改变场景中单个相机的位置得到或者使用固定于同一个平台的两个甚至多个相机采集得到。多相机系统具有体积大、成本高等缺点，并且每个相机的焦距、变焦程度、增益等光学特性略有不同，故所采集的立体图像的匹配点之间存在强度差异。研究人员使用单个相机和若干个光学器件的组合来实现立体视觉从而解决该技术问题，其中光学器件的核心功能为使单相机系统拥有不同的成像视角。Gao 等[3]通过旋转放置在单相机前的透明平板获得了立体图像。Teoh 等[4]将两个与光轴成 45° 的反射镜固定在相机两侧，同样通过旋转使相机前的第三个反射镜依次与两个固定镜平行从而获得了一对立体图像。然而，上述系统都需要解决旋转元件的精度问题。Lee 等[5]将双棱镜放置在相机前实现了立体图像采集，但需要使双棱镜的顶点与相机光轴严格平行，这样才能获取了一对尺寸相同的图像。Nene 等[6]提出了 4 种立体视觉系统，使用单个相机分别指向平面镜、椭球面镜、双曲面镜和抛物面镜。该系统依靠镜面反射在单相机上实现多视角，但需要复杂的镜像机制，由于多种曲率的反射镜设计，故难以实现系统的紧凑化。综上所述，寻求更直接的方法来实现结构更简单紧凑的单相机立体视觉系统具有重要的研究价值和意义。

自 Sato[7]于 1979 年提出了液晶透镜的概念以来，液晶透镜作为一种可电控调焦的光学器件在深度测量[8]、自动对焦[9-10]、增强现实[11]、虚拟现实[12]、景深扩展[13-14]和无偏成像[15]等领域中被广泛研究。一些液晶透镜除了电控调焦，还具有光轴移动功能。Masuda 等[16]利用分割圆孔电极的方法，实现了光束偏转。Ye 等[17-18]在此基础上提出了由多块图案化电极构成的液晶透镜结构，实现了焦点沿轴移动和离轴偏移。Ooba 等[19]提出了一种带有方形孔径的四电极可调液晶光阑。Kotova 等[20-21]利用文献[19]中的电极结构实现了液晶透镜，该透镜具有光轴移动功能。Zhang 等[22]提出了一种新的驱动方法，使文献[20]中的液晶透镜在变化焦距的过程中保持小像差。具有光轴移动功能的液晶透镜为在单相机系统上实现多视角成像提供了思路。

本文提出了一种新的单相机立体图像采集系统。利用光轴可移动液晶透镜的优势在于能够通过电控的方式实现对光轴的控制，从而在单相机上实现立体视觉，与通过旋转、镜面反射、三棱镜等各种方式实现多视角成像相比，其具有机制更简单的优势。同时，该液晶透镜可使系统在图像采集过程中不涉及机械移动，进而降低了系统的复杂性。液晶透镜轻薄且紧贴相机镜头，故系统紧凑，且制作成本低廉。通过干涉分析了

液晶透镜的光轴移动功能,建立模型研究了液晶透镜光轴变化对系统光轴的影响,以及视差与深度的关系,最后对利用光轴可移动液晶透镜实现的立体视觉进行了深度获取分析和说明。

2 基于光轴移动的立体视觉系统

2.1 液晶透镜

所用液晶透镜是一种基于模态控制的四电极较大口径液晶透镜[20-23],结构如图 1 所示,其中 $V_i(i=1,2,3,4)$ 为驱动电压幅值,并以有效区域中心为原点建立 xOy 坐标系。该透镜是由上下两块相同的具有矩形电极图案的氧化铟锡(ITO)玻璃基板和液晶层组成的三明治结构,两个玻璃基板内侧均镀有高阻抗层。高阻抗层通过磁控溅射 AZO 材料制成,其表面电阻率约为 10 MΩ/sq。液晶材料(江苏和成显示科技有限公司,137700-100 HTW)的双折射率之差为 $\Delta n=0.25$,寻常光分量的折射率为 $n_o=1.513$,非寻常光分量的折射率为 $n_e=1.774$,液晶层厚度为 50 μm,有效孔径(由上下两个大小为 2 mm×15 mm 的矩形刻蚀电极图案垂直交错构成)宽度 l 为 2 mm。玻璃基板厚度为 0.7 mm,液晶透镜整体厚度约为 1.6 mm。当模态控制参数满足一定关系时,高阻抗层内的电场近似线性分布[20]。在上下两个基板所产生的电场的线性叠加下,可实现已知中心对称分布的电场在液晶透镜有效区域内的任意移动。同时,为了呈现理想的透镜状态,液晶透镜中
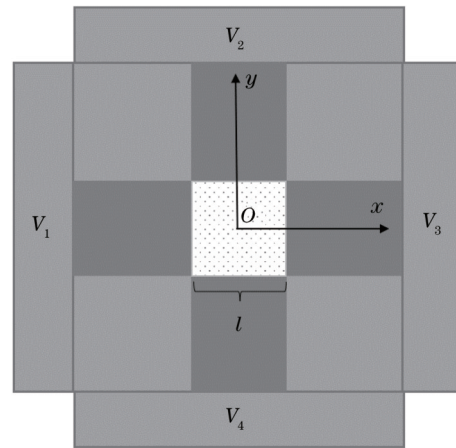
心的有效电压应保持为固定值,这样可使驱动电压和相位保持一定关系,从而实现成像质量的提高[22]。

图 1 液晶透镜俯视图
Fig. 1 Top view of liquid crystal lens

利用图 2 所示的 457 nm 波长的干涉光路测量了液晶透镜的特性,其中液晶透镜位于偏振方向相互垂直的两个偏振片之间,且摩擦方向与两个偏振片的任意一个偏振方向成 45°。图 3 展示了透镜有效区域内光轴水平移动时的干涉圆环图样。表 1 记录了这两个状态的驱动电压参数[干涉圆环的中心坐标,以及对应的驱动电压幅值和相位 $P_i(i=1,2,3,4)$],并将其用于后续图像采集中。
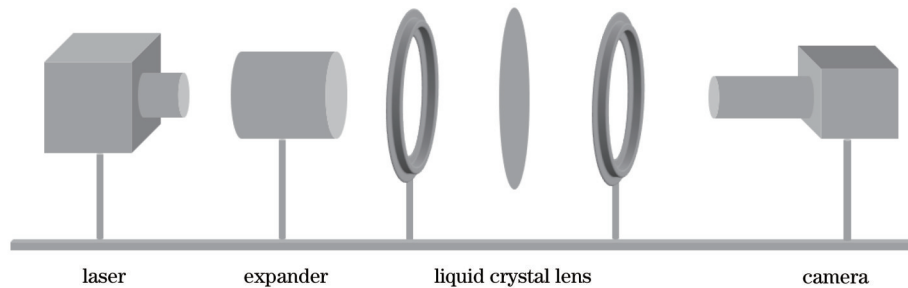

图 2 用于测试液晶透镜的偏振光干涉光路
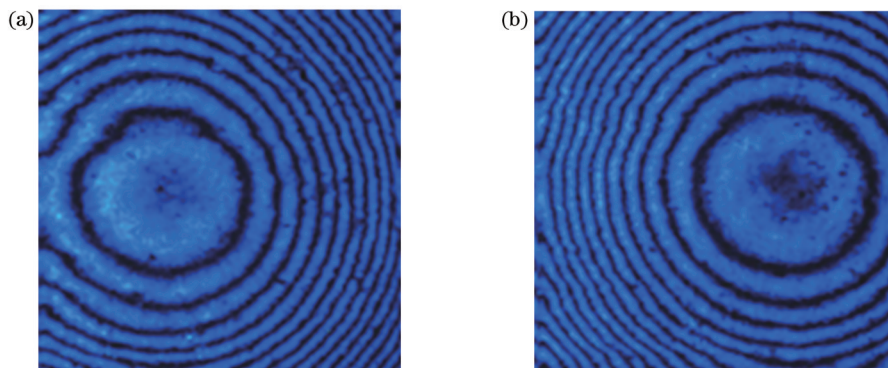Fig. 2 Polarized light interference path for testing liquid crystal lens

图 3 不同光轴位置的干涉结果。(a)光轴从(0,0)移动到(−0.4 mm,0);(b)光轴从(0,0)移动到(0.4 mm,0)
Fig. 3 Interference results for different optical axis positions. (a) Optical axis moving from (0, 0) to (−0.4 mm, 0); (b) optical axis moving from (0, 0) to (0.4 mm, 0)

表 1　两个光轴状态下液晶透镜的驱动电压参数

Table 1　Driving voltage parameters of liquid crystal lens in two optical axis states

Parameter	$(-0.4\ \mathrm{mm}, 0)$	$(0.4\ \mathrm{mm}, 0)$
V_1	0.51	0.77
V_2	0.63	0.63
V_3	0.77	0.51
V_4	0.63	0.63
$P_1\ /(°)$	0	0
$P_2\ /(°)$	0	0
$P_3\ /(°)$	90.01	90.01
$P_4\ /(°)$	95.00	95.00

液晶透镜处于正透镜状态,通过对干涉条纹进行分析得到了液晶透镜在图 3 所示的两个状态的均方根像差保持在 1/10 波长以下,光焦度保持为 $4.5\ \mathrm{m}^{-1}$。

2.2　成像系统

假设玻璃透镜的焦距为 f_g,光焦度为 $\phi_\mathrm{g}=1/f_\mathrm{g}$,由液晶透镜和玻璃透镜构成的组合镜头的光焦度为 $\phi=$ $\phi_\mathrm{g}+\phi_\mathrm{LC}-d\phi_\mathrm{g}\phi_\mathrm{LC}$,其中 ϕ_LC 为液晶透镜的光焦度,d 为液晶透镜与玻璃透镜之间的距离,且 $\phi_\mathrm{g}>\phi_\mathrm{LC}$。如图 4 所示,选取两条特殊光线对成像系统进行分析。c_1 和 c_2 分别表示液晶透镜和玻璃透镜的光轴位置,δ 为通过调整电压实现的液晶透镜光轴的移动量。其中一条光线与液晶透镜的光轴重合,到达玻璃透镜表面并被折射后穿过焦点 F'_g,另一条平行光线被液晶透镜折射后穿过玻璃透镜的光心到达焦点 F'_LC,这两条光线的交点即为成像系统的焦点。以 F'_g 为坐标原点建立坐标系,求解两条光线通过玻璃透镜后的轨迹方程可得到交点 F 坐标的 y 分量为 $f'_\mathrm{g}\delta/(f'_\mathrm{LC}+f'_\mathrm{g}-d)$。该分量是液晶透镜光轴移动 δ 后整个成像系统的等效光轴移动量(记为 Δc),故成像系统在像面上得到的图像移动量为 $\Delta y'=\Delta c+|\beta|\Delta c$,其中 β 为系统的垂轴放大率,由 $1/v-1/u=\phi$ 可得到 $\beta=1-\phi v$,说明不同物点在经过该成像系统后有不同的图像移动量,其中 v 为像距,u 为物距,ϕ 为透镜组光焦度。将液晶透镜的光圈作为成像系统的孔径光阑。
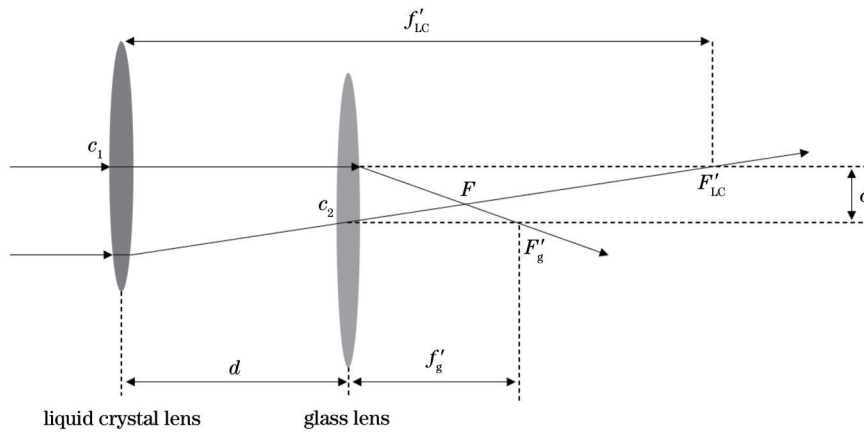

图 4　成像系统光学模型

Fig. 4　Optical model of imaging system
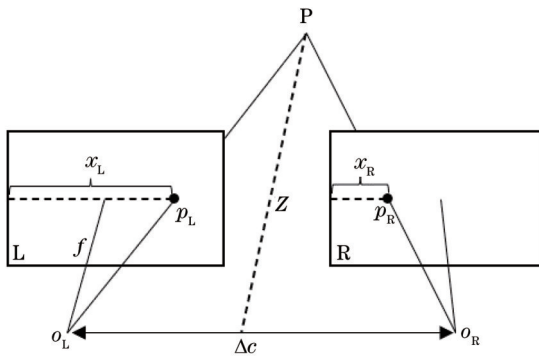
将成像系统的两个等效光轴状态模型简化为图 5 所示的针孔相机模型,从中可以得到视差与深度的关系。

对于同一个物点 P,将光轴移动前后在像面上得到的图像分别标记为 L 和 R。根据几何相似关系

$$\frac{\Delta c-(x_\mathrm{L}-x_\mathrm{R})}{\Delta c}=\frac{Z-f}{Z}, \tag{1}$$

得到深度与视差的关系

$$Z=\frac{f\Delta c}{x_\mathrm{L}-x_\mathrm{R}}, \tag{2}$$

式中:$x_\mathrm{L}-x_\mathrm{R}$ 表示 P 点在 L 和 R 两幅图像上的视差;$f=1/\phi$ 为成像系统的组合焦距。

光流是空间物体的瞬时运动速度在图像平面上的投影,当两张图像的光流结果的方向具有一致性而大小具有差异性时,光流结果体现了这两张图像所包含的视差信息。本文图像是在单相机固定不动的前提下利用液晶透镜的光轴水平移动采集得到的,故像素移动方向具有一致性,而物体前后位置不同进而又具有

图 5　基于光轴移动的针孔相机模型

Fig. 5　Pinhole camera model based on optical axis movement

像素位移量的差异性。Brox 等[24]基于变分框架的光流法具有亚像素的光流计算精度且算法鲁棒性好，在模型上添加了具有丰富信息的区域匹配项，解决了图像序列中小结构物体快速移动的光流计算问题。本文使用变分光流法计算图像位移量差异，从而对图像包含的视差信息进行提取。

3 实验结果

实验装置由一个相机、一个焦距为 35 mm 的镜头和一个液晶透镜组成。玻璃镜头的筒长为 2 cm，液晶透镜整体厚度为 1.6 mm，且紧贴着玻璃镜头，液晶镜上贴有一个偏振片，其偏振方向与液晶透镜玻璃基板的摩擦方向一致。相机（广州市明美科技有限公司，MD50-T）的像素大小为 2.2 μm，分辨率为 2592 pixel×1944 pixel。系统的实物装置如图 6 所示，其中玻璃镜头前方为液晶透镜的固定架。
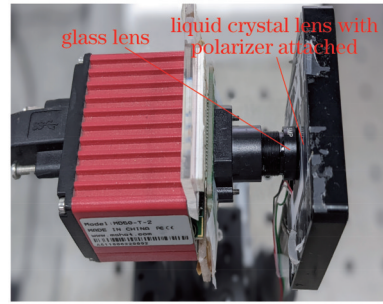
在实验中，三个物体被放置在如图 7 所示的不同

图 6 所设计系统的实物装置图
Fig. 6 Physical device diagram of designed system

位置。先将相机对焦在背景板上，对液晶透镜施加电压使 e 光被调制，原本对焦清晰的地方此时出现离焦，再利用液晶透镜的电控调焦功能将系统的对焦点调整到中间物体上。在图 3 所示的两个光轴状态下进行图像采集，可得到如图 8(a)、(b)所示的两张图像。图 8 (c)展示了液晶透镜在不同光轴状态下同一区域图像的差异，如 8(a)、(b)中的矩形框区域所示。
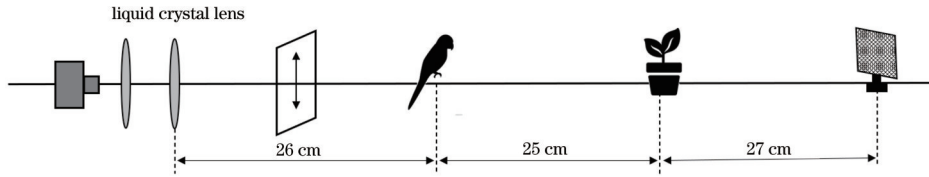

图 7 基于液晶透镜光轴移动的实验装置图
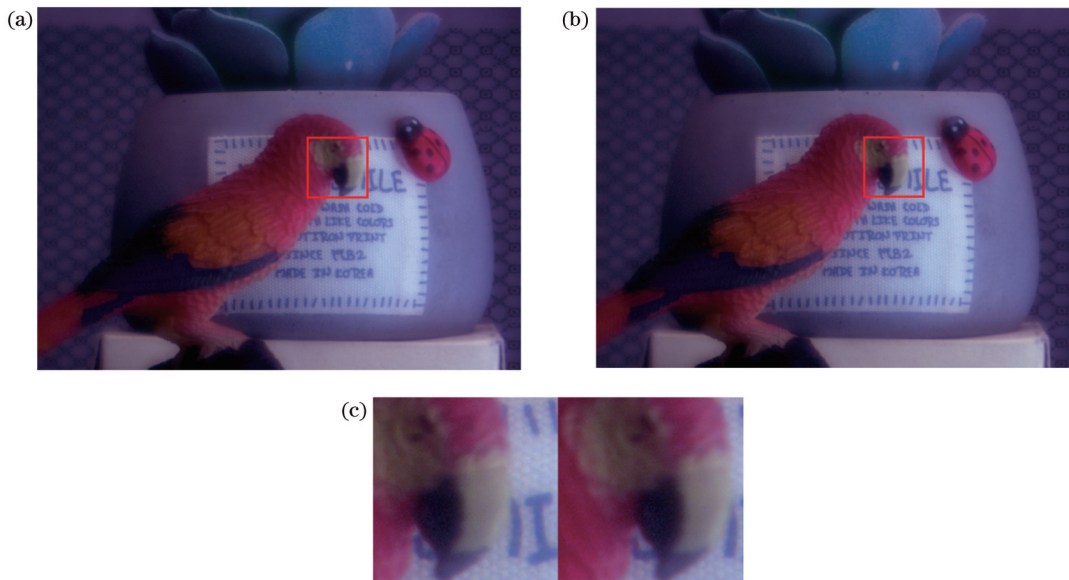Fig. 7 Experimental setup based on movement of optical axis of liquid cystal lens

图 8 基于液晶透镜光轴移动的图像采集结果。(a)液晶透镜光轴位于(−0.4 mm,0)处的采集结果；(b)液晶透镜光轴位于(0.4 mm,0)处的采集结果；(c)图 8(a)、(b)中矩形框区域图像对比
Fig. 8 Image acquisition results based on optical axis movement of liquid crystal lens. (a) Acquisition result for liquid crystal lens with optical axis at (−0.4 mm, 0); (b) acquisition result for liquid crystal lens with optical axis at (0.4 mm, 0); (c) comparison of images in rectangular box areas from Figs. 8(a) and 8(b)

光流计算结果如图 9 所示。算法结果中同种颜色表示同一像素的移动方向，颜色越深则像素移动量越

大，对应的视差越大。
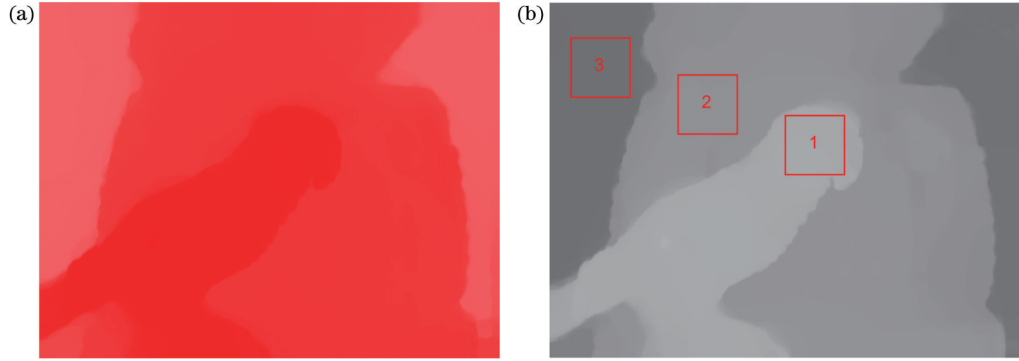
选取图 9(b)所示的三个 161 pixel×161 pixel 区域

图 9　基于变分光流法的视差结果。(a)光流结果原图；(b)经过灰度化取反的光流结果

Fig. 9　Disparity results based on variable optical flow algorithm. (a) Original image of optical flow result; (b) optical flow result after grayscale inversion

进行平均灰度分析，将平均灰度值和物体的实际距离汇总在表 2 中。图 10 为实际距离值与平均灰度值的线性拟合，可以发现视差的大小与物体的距离成反比关系，验证了利用所设计的成像系统采集物体视差信息的可行性。

表 2　图 9(b)中矩形框区域的平均灰度和对应的实际距离值

Table 2　Average grayscale values of rectangular box areas in Fig. 9 (b) and corresponding actual distance values

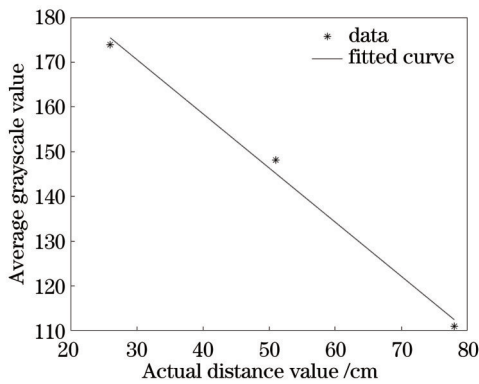| Region of interest No.	1	2	3
Average grayscale value	173.1	148.6	111.0
Actual distance value /cm	26.0	51.0	78.0

图 10　实际距离值与平均灰度值的拟合关系

Fig. 10　Fitting relationship between actual distance value and average grayscale value

设置近距离实验，调整物距，其中左侧、中间和右侧的卡片与液晶透镜的距离分别为 6.5 cm、7.6 cm 和 9.1 cm。其余参数与图 7 所示实验一致。

由于液晶透镜紧贴玻璃透镜，故假设 $d=0$。像元尺寸为 2.2 μm，光流大小与像元尺寸的乘积为图像上物体的移动量。记录图 11(d)中三个框选区域的平均灰度值和实际光流大小，利用式(2)计算物体的深度信息，将所有数据汇总于表 3 中。

根据双目测距原理，基线距离越大，精度越高，可测量距离越远。不同双目测距系统在同一基线距离下

表 3　深度获取实验数据汇总

Table 3　Summary of depth measurement experimental data

Region of interest No.	1	2	3
Average grayscale value	177.0	156.4	144.9
Optical flow value /pixel	25.6	22.2	20.4
Calculated depth value /cm	5.9	6.8	7.4
Actual distance value /cm	6.5	7.6	9.1
Error in result /%	9.2	10.5	18.7

采集的图像实际含有的视差信息是一致的，但通过算法获取的视差是有误差的，从而会产生深度信息的精度差别。利用双目视觉经典算法 SGM(semi-global matching)[25]和 SAD(sum of absolute differences)将图 11(a)、(b)作为输入进行视差计算，得到的结果如图 12(a)、(b)所示。

可以看出，传统双目视觉算法 SGM 和 SAD 无法获取小基线立体视觉系统所采集的图像的有效视差，故无法恢复出有意义的深度信息。然而，光流法可以获取丰富的视差信息，如图 11(d)所示。在图像的移动方向具有一致性的前提下，视差就是计算同一特征点在两张图像上的像素移动量，这与光流矢量的大小是一致的。所设计系统被证明工作状况良好，但因基线距离小，故只能获取近距离物体的深度信息，在进行视差计算时需要配合高精度的变分光流算法，深度计算误差随着物距的增大而增大。

4　结　　论

提出了一种立体图像采集系统，并对液晶透镜的结构和光轴移动特性进行了说明。首先，利用液晶透镜光轴可移动实现了成像系统的整体光轴平移，完成了含有场景视差信息的立体图像采集。然后，利用光流法完成了图像视差的提取，并进行了近距离物体的深度获取实验。相比于通过改变场景中单个相机的位置或使用固定于同一平台的多个相机的传统图像采集方式，所设计系统在采集时仅使用单个相机且无需机械移动，具有机制简单、系统紧凑等优点，可使用变分
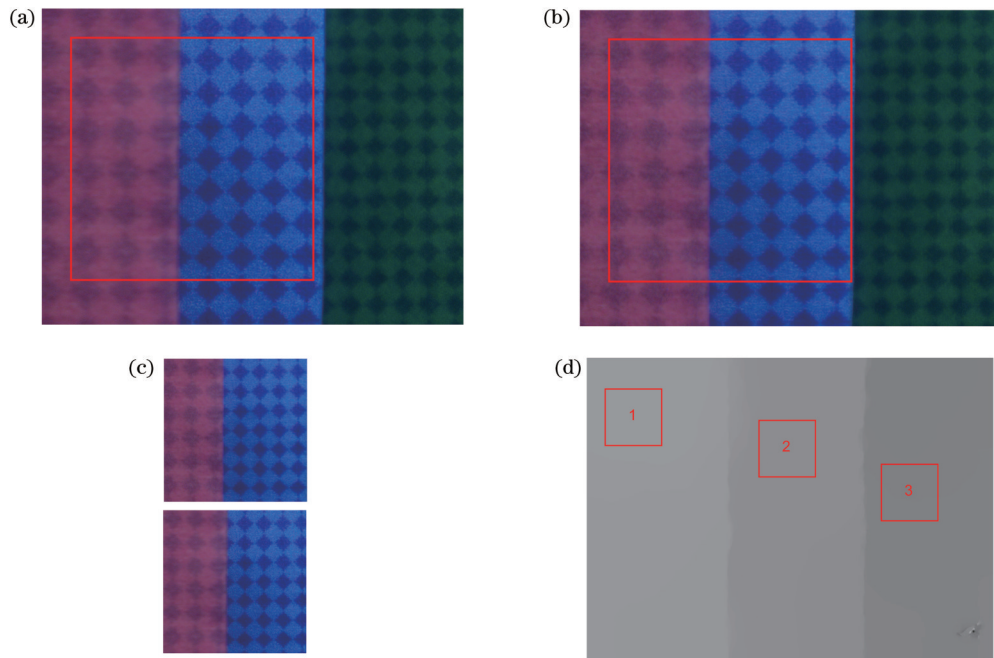
图 11　近距离物体的深度获取实验。(a)液晶透镜光轴位于(−0.4 mm，0)处的采集结果；(b)液晶透镜光轴位于(0.4 mm，0)处的采集结果；(c)图8(a)、(b)中矩形框区域图像对比；(d)光流法的灰度化视差结果

Fig. 11　Depth measurement experiment of close range object. (a) Acquisition result for liquid crystal lens with optical axis at (−0.4 mm，0); (b) acquisition result for liquid crystal lens with optical axis at (0.4 mm，0); (c) comparison of images in rectangular box areas from Figs. 11(a) and 11(b); (d) grayscale disparity result based on optical flow algorithm
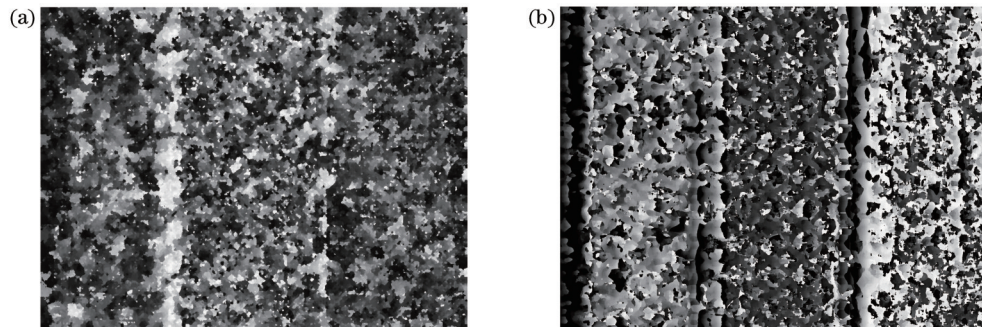

图 12　传统双目视觉算法对小基线图像的处理结果。(a) SGM；(b) SAD

Fig. 12　Results of small baseline images obtained by conventional binocular vision algorithms. (a) SGM；(b) SAD

光流法从光轴水平移动获取的图像对中恢复物体的深度信息。

参 考 文 献

[1] Yu Q H, Liu H, Sun S L. Optical design of an off-axis telescope: large aperture, small f/number, wide FOV[J]. Proceedings of SPIE, 2008, 7100: 71001X.

[2] Nakhaeinia D, Tang S H, Noor S B M, et al. A review of control architectures for autonomous navigation of mobile robots [J]. International Journal of Physical Sciences, 2011, 6(2): 169-174.

[3] Gao C Y, Ahuja N. Single camera stereo using planar parallel plate[C]//Proceedings of the 17th International Conference on Pattern Recognition, August 26, 2004, Cambridge, UK. New York: IEEE Press, 2004: 108-111.

[4] Teoh W, Zhang X. An inexpensive stereoscopic vision system for robots[C]//Proceedings of 1984 IEEE International Conference on Robotics and Automation, March 13-15, 1984, Atlanta, GA, USA. New York: IEEE Press, 1984: 186-189.

[5] Lee D, Kweon I S. A novel stereo camera system by a biprism [J]. IEEE Transactions on Robotics and Automation, 2000, 16(5): 528-541.

[6] Nene S A, Nayar S K. Stereo with mirrors[C]//Sixth International Conference on Computer Vision, January 7, 1998, Bombay, India. New York: IEEE Press, 1998: 1087-1094.

[7] Sato S. Liquid-crystal lens-cells with variable focal length[J]. Japanese Journal of Applied Physics, 1979, 18(9): 1679-1684.

[8] Ye M, Chen X X, Li Q C, et al. Depth from defocus measurement method based on liquid crystal lens[J]. Optics Express, 2018, 26(22): 28413-28420.

[9] Galstian T, Sova O, Asatryan K, et al. Optical camera with liquid crystal autofocus lens[J]. Optics Express, 2017, 25(24): 29945-29964.

[10] 兰天成，兰荣华，陈晓西，等. 液晶透镜爬山自动对焦算法研究[J]. 光学学报，2020，40(14): 1411003.
Lan T C, Lan R H, Chen X X, et al. Research on liquid crystal lens hill climbing autofocus algorithm[J]. Acta Optica Sinica, 2020, 40(14): 1411003.

[11] Chen H S, Wang Y J, Chen P J, et al. Electrically adjustable location of a projected image in augmented reality via a liquid-crystal lens[J]. Optics Express, 2015, 23(22): 28154-28162.

[12] Lin Y H, Huang T W, Huang H H, et al. Liquid crystal lens set in augmented reality systems and virtual reality systems for rapidly varifocal images and vision correction[J]. Optics Express, 2022, 30(13): 22768-22778.

[13] Bai Y C, Chen X X, Ma J C, et al. Transient property of liquid crystal lens and its application in extended depth of field imaging[J]. Optics Communications, 2020, 473: 125974.

[14] 刘志强，胡轶瑶，叶茂. 液晶轴棱锥[J]. 光学学报，2022，42(8): 0823001.
Liu Z Q, Hu Y Y, Ye M. Liquid crystal axicon[J]. Acta Optica Sinica, 2022, 42(8): 0823001.

[15] 李鹏伟，陈信慈，陈晓西，等. 用90°扭曲向列相液晶盒代替偏振片的液晶透镜成像方法[J]. 光学学报，2022，42(7): 0711004.
Li P W, Chen X C, Chen X X, et al. Liquid crystal lens imaging method using 90° twisted nematic liquid crystal cell instead of polarizer[J]. Acta Optica Sinica, 2022, 42(7): 0711004.

[16] Masuda S, Takahashi S, Nose T, et al. Liquid-crystal microlens with a beam-steering function[J]. Applied Optics, 1997, 36(20): 4772-4778.

[17] Ye M, Sato S. Liquid crystal lens with focus movable along and off axis[J]. Optics Communications, 2003, 225(4/5/6): 277-280.

[18] Ye M, Wang B, Sato S. Liquid crystal lens with focus movable in focal plane[J]. Optics Communications, 2006, 259(2): 710-722.

[19] Ooba Y, Sugihara S, Shiwa S. Basic study of A bright area-modulative liquid crystal cell[J]. Proceedings of SPIE, 1986, 0639: 47-55.

[20] Kotova S P, Patlan V V, Samagin S A. Tunable liquid-crystal focusing device. 1. Theory[J]. Quantum Electronics, 2011, 41(1): 58-64.

[21] Kotova S P, Patlan V V, Samagin S A. Tunable liquid-crystal focusing device. 2. Experiment[J]. Quantum Electronics, 2011, 41(1): 65-70.

[22] Zhang Y L, Li G Y, Chen X X, et al. Driving methods for liquid crystal lens with rectangular aperture and four voltages[J]. Japanese Journal of Applied Physics, 2021, 60(10): 102002.

[23] Xu L H, Zhang Y L, Liu Z Q, et al. Liquid crystal lens with four driving voltages and its applications in imaging system with rectangular aperture[J]. Japanese Journal of Applied Physics, 2022, 61(2): 028001.

[24] Brox T, Bruhn A, Papenberg N, et al. High accuracy optical flow estimation based on a theory for warping[M]//Pajdla T, Matas J. Computer vision-ECCV 2004. Lecture notes in computer science. Heidelberg: Springer, 2004, 3024: 25-36.

[25] Hirschmuller H. Accurate and efficient stereo processing by semi-global matching and mutual information[C]//2005 IEEE Computer Society Conference on Computer Vision and Pattern Recognition, June 20-25, 2005, San Diego, CA, USA. New York: IEEE Press, 2005: 807-814.

Stereo Image Acquisition System Using Optical Axis Movable Liquid Crystal Lens

Wan Chaojie[1], Liu Zhiqiang[1], Xu Lühan[1], Li Huihai[2], Ye Mao[1*]

[1]*School of Optoelectronic Science and Engineering, University of Electronic Science and Technology of China, Chengdu 611731, Sichuan, China;*
[2]*Sichuan Tianwei Electronics Co., Ltd., Chengdu 610200, Sichuan, China*

Abstract

Objective　Stereo images are usually acquired by changing the position of a single camera in the scene or by using two or even more cameras fixed at the same platform. Multi-camera systems are large and costly, and due to slight differences between each camera in terms of focal length, zoom level, camera gain, and so on, there are inevitable intensity differences between the matching points of the stereo images. Researchers have adopted methods combining a single camera and several optics devices to achieve stereo vision, so as to avoid this problem. The core function of the optics devices is to develop a single camera system with different imaging views. Various optical components have been reported in studies, for example, by rotating a flat glass plate or some plane mirrors placed in front of a single camera, or using a single camera pointing at a biprism or some multiple parabolic mirrors. However, optics rotation systems need to address the accuracy of mechanical movement, and biprism systems need to solve the problem of how to get the same image size. Parabolic mirror systems using multiple curvatures involve complex mirroring mechanisms, and the mirrors with multiple curvatures make the system difficult to be compact. Therefore, it is of research value and significance to seek more direct methods to realize a single-camera stereo vision system with a simpler and more compact structure. In this study, a single-camera stereo image acquisition system using an optical axis movable liquid crystal lens is presented. The optical axis position of the liquid crystal lens can be controlled by adjusting the voltage, and thus the stereo vision in a single camera can be achieved. Although it is consistent with the purpose of multi-view imaging through rotation, mirror reflection, biprism, etc., the mechanism of the designed system is simple. It allows the system to be used without mechanical movement during image acquisition, so as to reduce the complexity of the system. The liquid crystal lens is thin and light, and fits closely to the camera lens, which makes the system compact and enables a low cost.

Methods　　The system consists of a fixed camera module and a liquid crystal lens with a polarizer attached. First, the structure of the liquid crystal lens is described, and a polarized interference optical path is built to analyze optical axis movement properties, including the magnitude of the motion at the corresponding drive voltage as well as the aberration and optical power. Then, the effect of the optical axis position change of the liquid crystal lens on the overall system is analyzed, and the relationship between disparity and depth is derived through the pinhole camera model. Finally, the system is used to acquire stereo images, and the disparity is calculated by the optical flow algorithm. The depth information of the scene is inferred from the disparity information in the close-range experiment, and error analysis is performed. In addition, the problems of other disparity acquisition algorithms in the designed system are illustrated.

Results and Discussions　　The proposed single-camera system using an optical axis movable liquid crystal lens is proved to have a stereo vision effect. The images in this paper are acquired by using the horizontal movement of the optical axis of the liquid crystal lens while the single camera is fixed. The images have consistent direction of pixel movement and variation in the amount of pixel shift depending on the object distance. At this point, the disparity is the same magnitude as the optical flow. Therefore, the difference in the amount of pixel movement by using the optical flow algorithm is calculated, and dense disparity information is obtained [Fig. 9(b)]. It indicates that the system can capture disparity information about the scene (Fig. 10). Depth of objects is inferred back from the disparity in the close-range experiment (Table 3). The baseline distance in this system is small, and conventional stereo vision algorithms such as semi-global matching (SGM) and sum of absolute differences (SAD) are unable to acquire dramatic disparity information on the images acquired by the system (Fig. 12). According to the binocular distance measuring principle, as the baseline distance becomes greater, higher accuracy and longer distance that can be measured. It has been proven that the designed system works well, and it can acquire dense disparity information through the optical flow algorithm and allow the depth measurement of objects at close range with some accuracy.

Conclusions　　In this study, a stereo image acquisition system is proposed. The system consists of a fixed camera module and a liquid crystal lens with a polarizer attached. We adjust the voltage to move the optical axis of the liquid crystal lens, capture images, and use optical flow algorithm to obtain disparity information. In addition, we analyze the effect of the optical axis movement of the liquid crystal lens on the overall optical axis of the system, and derive the relationship between the disparity and the depth. In the experiment, the feasibility of the system is demonstrated by verifying the existence of the disparity in the acquired images, and depth acquisition of close-range objects is performed. Experimental results show that the optical axis movement function of the liquid crystal lens can be used to move the overall optical axis of the system to achieve stereo vision. The designed system does not require any mechanical movement, and features a simple and compact structure and a low cost. Therefore, it provides a new method for the acquisition of stereo images.

Key words　　imaging systems; liquid crystal lenses; optical axis movement; image acquisition; depth measurement